Spectroelectrochemical Signatures of Capacitive Charging and Ion Insertion in Doped Anatase Titania Nanocrystals

Clayton J. Dahlman,[1] Yizheng Tan,[1,2] Matthew A. Marcus,[3] Delia J. Milliron[1,*]

1. McKetta Department of Chemical Engineering, 200 E. Dean Keeton Street, The University of Texas at Austin, Texas 78712, USA

2. The Molecular Foundry, Lawrence Berkeley National Laboratory, 1 Cyclotron Rd., Berkeley, California 94720, USA

3. The Advanced Light Source, Lawrence Berkeley National Laboratory, 1 Cyclotron Rd., Berkeley, California 94720, USA

*Electronic address: *milliron@che.utexas.edu*

Supporting Information.

Nb-TiO_2 Nanocrystal Synthesis.

The synthesis of niobium-doped anatase TiO_2 (Nb-TiO_2) nanocrystals (NCs) was adapted from de Trizio *et al.*[1], with slight modifications. For both the Nb-doped and undoped TiO_2 NCs, a mixture of oleic acid (2 mmol) and oleyl alcohol (26 mmol) in octadecene (ODE, 8 mL) was degassed under vacuum at 120°C for 1 hour in a three-neck flask. A solution of niobium pentachloride ($NbCl_5$) in ODE (2 mL) was stirred and heated to 80°C under nitrogen atmosphere for one hour to dissolve the precursor. After one hour of heating the $NbCl_5$ in ODE solution, titanium ethoxide (TEO, 2 mmol) was added creating a clear solution. Immediately after adding TEO, the precursor solution was rapidly injected via a syringe into the degassed solvent of the three-neck flask, under nitrogen atmosphere. The temperature of the reaction vessel was then raised to 290°C for 60 minutes to grow the TiO_2 NCs. After cooling to room temperature, the NC solution was washed by precipitation with acetone and redispersion in hexane, repeated four times. After each precipitation, 100μL of oleic acid was added to the NC solution to stabilize the colloidal particles. The final NC solution was prepared by redispersing the particles in 2mL of

hexane and 15μL of oleic acid. Nb doping content is expressed as the percentage of Ti sites occupied by Nb in the anatase structure. The Nb to Ti ratio was measured by digesting NC solutions for one day in a concentrated aqueous solution of 10:1 HCl to HNO_3. Inductively Coupled Plasma-Optical Emission spectra of the digested solutions were obtained with a Varian ICP-OES 720 Series spectrometer to calculate the Nb:Ti ratio.

Electron Microscopy.

Low-resolution TEM were measured on a Libra 120 microscope operating at 120kV. SEM were measured on a Hitachi S-5500 STEM operating at 5.0kV in Secondary Electron mode.

Film Deposition.

Conductive mesoporous films of colloidal TiO_2 NCs were prepared by spin coating and annealing solutions of ligand-stripped NCs. The oleic acid ligands bound to the surface of the colloidal NCs upon synthesis were removed, according to a procedure adapted from Dong *et al.*[2], by adding the NC solution to a two-phase mixture of N,N-dimethylformamide (DMF) and hexane. Then, roughly 1 mg of nitrosonium tetrafluoroborate ($NOBF_4$) was added and the resulting mixture was sonicated for 30 minutes, or until complete phase segregation of the ligand-stripped NCs was achieved. The NCs, now free of organic capping ligands and weakly coordinated to DMF molecules, were washed by precipitation with toluene and redispersion in DMF, repeated three times. A final NC solution of roughly 60 mg TiO_2 mL^{-1} in a 4:1 mixture of acetonitrile:DMF was prepared from the ligand stripped particles. For film deposition on either ITO-coated glass or silicon wafers, the substrate was first washed in chloroform, then acetone, then isopropanol to improve film adhesion. Films of roughly 100-200nm were prepared by spin coating the polar NC solution on the cleaned substrates, followed by annealing under Argon for 30 minutes at 300°C to remove organics. The most uniform films were obtained by preparing films immediately after ligand stripping. The thickness and uniformity of the TiO_2 films were measured with a Veeco Dektak 150 profilometer.

Electrochemistry.

Electrochemical measurements were taken with a Biologic VMP3 potentiostat. *In situ* transmission spectra were recorded through the NC film working electrode an ASD LabSpec4 spectrometer across a spectral window of 400-2200 nm, limited by strong absorption bands from the liquid electrolytes. Both intercalating (LiTFSI) and non-intercalating (TBATFSI) electrolyte salts were vacuum baked at 150°C for 12 hours, and tetraglyme was dried with a molecular sieve, to remove residual water prior to preparing the electrolyte solutions. For experiments using a fixed applied potential, the working electrode was held at the applied potential until the current equilibrated to a constant value due to a minor leakage current, usually after a time span of roughly one hour.

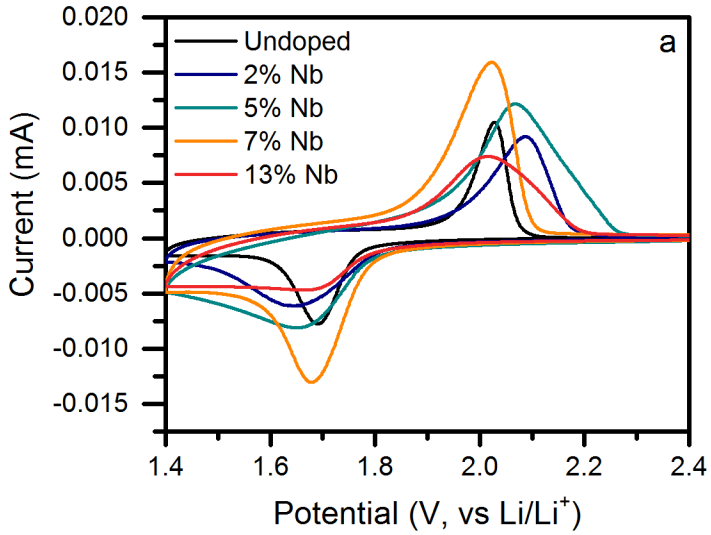

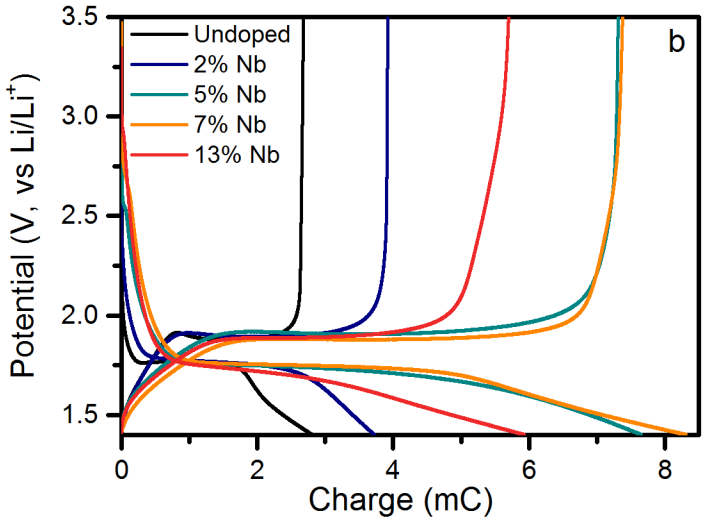

Figure S1. A series of Nb-TiO_2 NC films were tested in a) cyclic voltammetry at 0.5 mV/s and b) galvanostatic charging experiments at a rate of roughly 1C measured empirically from CV data in a). The electrolyte was 0.1M LiTFSI in tetraglyme. All films were had a thickness of 130nm ± 35nm and charged within a constant-area (0.5 cm^2) cell sealed by an O-ring inside an argon glovebox.

Phase Transitions upon Lithiation.

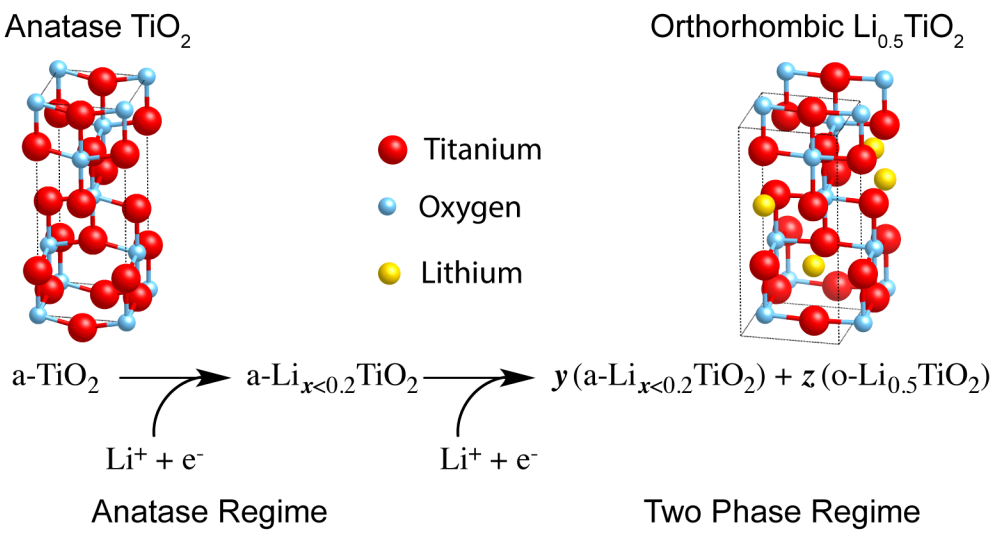

Figure S2. A discrete phase change from anatase to orthorhombic $Li_{0.5}TiO_2$ occurs upon sufficient lithiation, resulting in a two-phase regime.

X-Ray Diffraction.

The XRD patterns shown in Figure 3 show phase transitions upon reduction during a single charging cycle. The patterns shown below, in Figure S3, show phase behavior upon charging and discharging for two cycles. The phase transition is clearly reversible for both anatase and 10% Nb-TiO_2 NC films. The noisy patterns for as-deposited undoped TiO_2 and the sharp peak at 2.3$Å^{-1}$ are attributed to experimental noise from the baselining procedure used to subtract silicon diffraction from the TiO_2 NC patterns. Transmission and grazing incidence XRD patterns were collected with a 2D area detector, and diffraction patterns were averaged across the measured range of the 2D detector, i.e. assuming isotropic scattering. The beam energy for transmission WAXS was calibrated using a reference sample of LaB_6, and had a wavelength of 0.9744Å. The detector distance was 200mm.

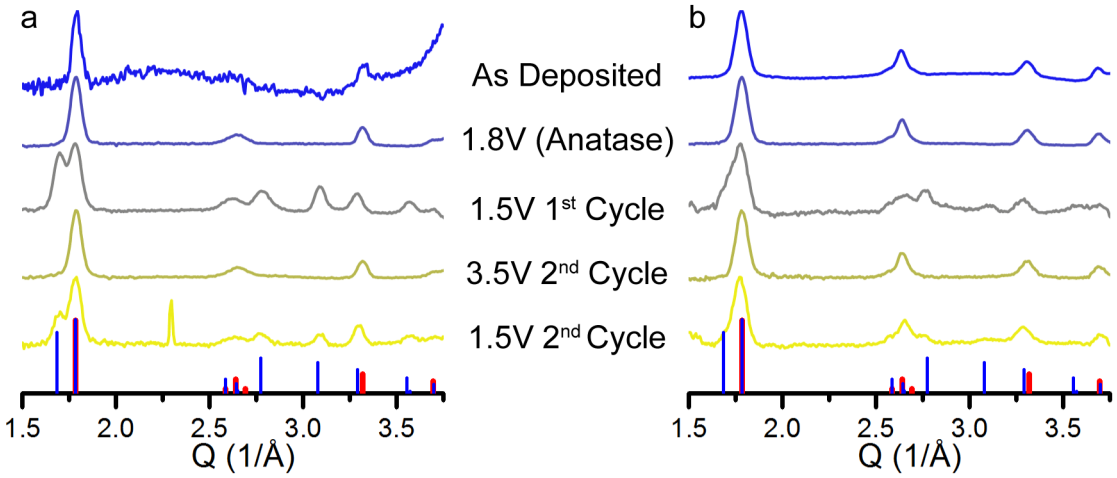

Figure S3. Transmission wide-angle XRD spectra are shown for a) undoped and b) 10% Nb-TiO_2 NC films, for a range of electrochemical charging potentials. Films were electrochemically cycled in 0.1M LiTFSI in tetraglyme. The as-deposited and partially-reduced 1.8V patterns match the anatase structure ($I4_1$/amd, ICSD Coll. Code 96946, red), and the fully reduced 1.5V pattern corresponds to the $Li_{0.5}TiO_2$ phase (Imma, ICSD Coll. Code 96948, blue), reported for microscale anatase TiO_2[3].

A second series of synchrotron XRD experiments were performed at beamline 11-3 of SSRL in grazing incidence mode to observe the phase transitions of the NC film upon oxidation, as shown in Figure S4. Films were deposited on a silicon substrate coated with 10nm of gold, and electrochemically charged by the same method as described for the transmission WAXS samples. Charged films were then transferred air-free to a helium-filled glovebag attached to an enclosed, helium-atmosphere sample chamber. XRD spectra were recorded in grazing incidence geometry with an incident angle of 0.12 degrees to the substrate surface. The beam energy for GIWAXS was calibrated using a reference sample of LaB_6, and had a wavelength of 0.9744Å. The detector distance was 150mm. The GIWAXS spectra have much broader peaks than the transmission mode data, but there is still clear evidence of a discrete phase change that occurs across the 1.8V lithiation threshold. In the oxidative direction, the 1.8V spectra for all four samples (red lines) have peaks that correspond to the orthorhombic $Li_{0.5}TiO_2$ phase, and match the profile of the 1.5V reduced spectra. However, the oxidative 1.8V spectra are all broader than

the 1.5V spectra, with some evidence of delithiation, indicating that there may be a partial transition to anatase upon oxidation from 1.5V to 1.8V.

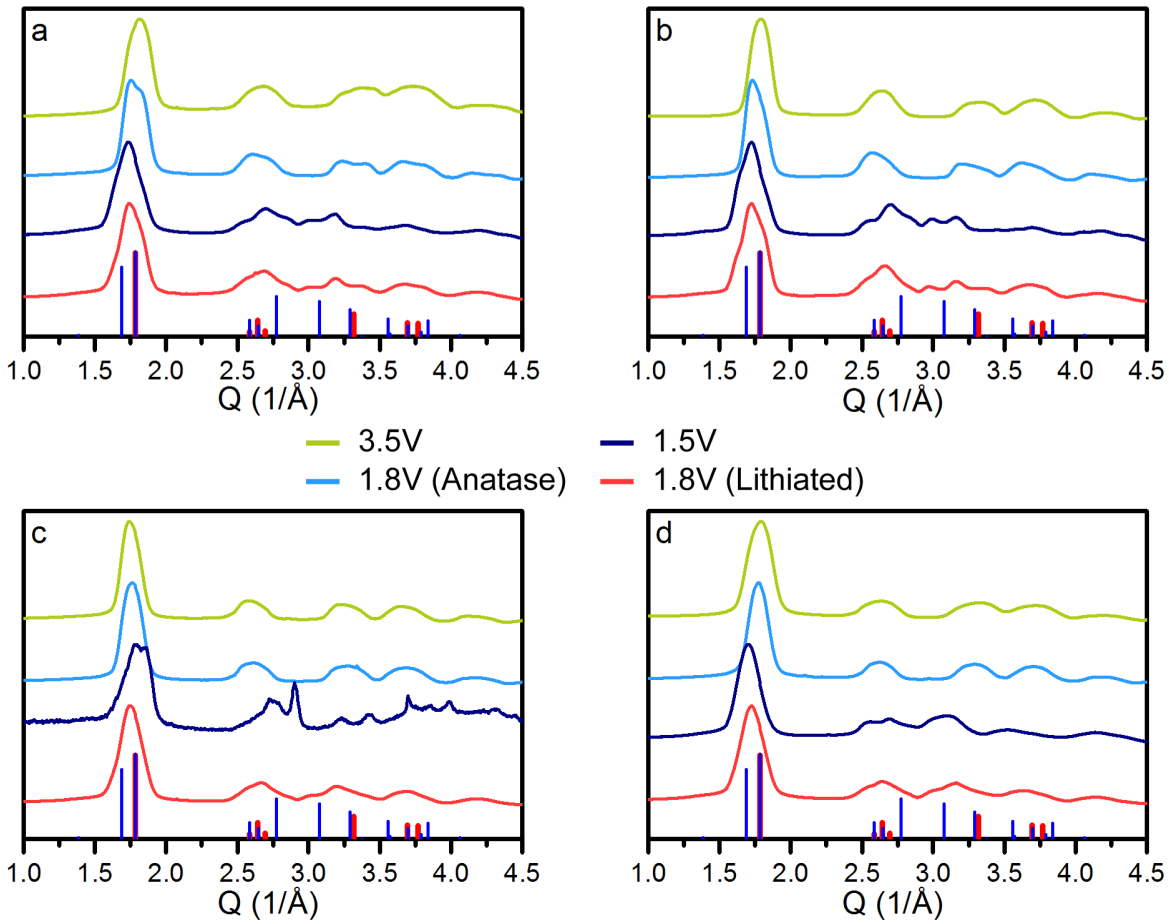

Figure S4. Grazing-Incidence wide angle XRD spectra are shown for a) undoped, b) 2.5% Nb, c) 9% Nb and d) 19% Nb-TiO_2 NC films, electrochemically charged to four different potentials. Films were electrochemically cycled in 0.1M LiTFSI in tetraglyme. The as-deposited and partially-reduced 1.8V patterns match the anatase structure ($I4_1$/amd, ICSD Coll. Code 96946, red), and the fully reduced 1.5V and partially-oxidized 1.8V patterns correspond to the $Li_{0.5}TiO_2$ phase (Imma, ICSD Coll. Code 96948, blue), reported for microscale anatase TiO_2[3].

X-Ray Absorption Spectroscopy.

The XANES pre-edge spectra in Figures 5 and 6 were obtained from full Ti K-edge XAS spectra at beamline 10.3.2 of ALS. Energy was calibrated by measuring transmission X-Ray absorption through a titanium foil, and by fitting the maximum of the first derivative at the Ti K-

edge to 4966.4 eV[4]. More details about the beamline are reported by Marcus *et al*[5]. The main edge features and extended structures are presented in Figure S5 below. The edge shift upon electrochemical lithiation is clearly visible in the undoped TiO_2 charging experiment, along with changes in the extended structure, as expected for a bulk phase transition. Nb-TiO_2 charging experiments yielded similar results. A comparison of the as-deposited XAS spectra of the Nb-TiO_2 NCs reveals that there is a slight deviation in the extended structure and peak profiles for high doping contents. However, there is no appreciable shift in the main edge energy upon any level of Nb doping, as shown in the first derivative plot (Figure S5c).

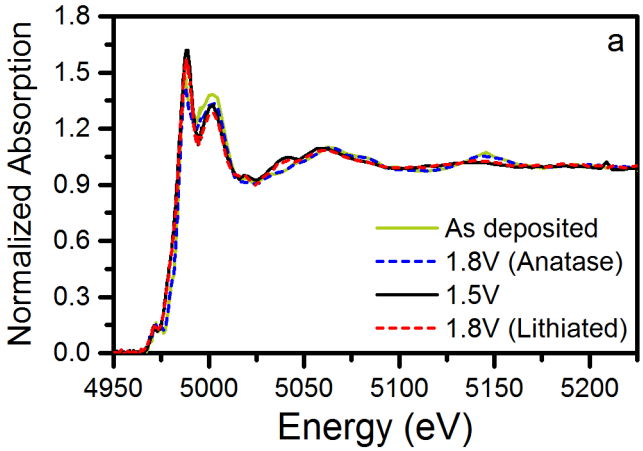

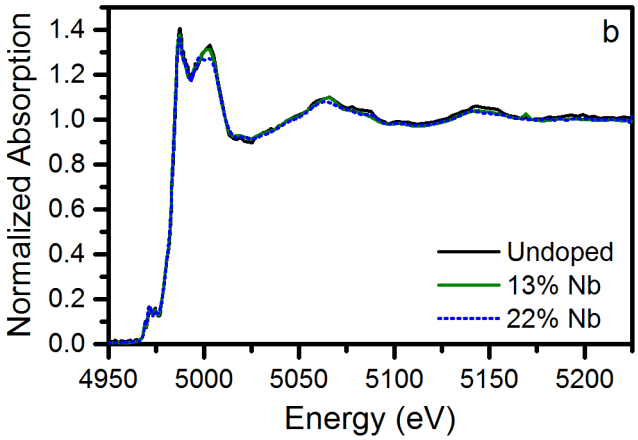

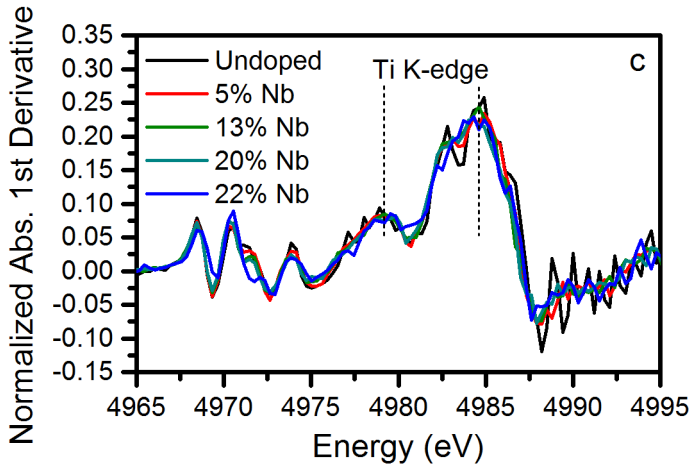

Figure S5. X-Ray Absorption Spectra at the Ti K-edge of a) undoped TiO_2 NC films electrochemically charged to a range of potentials, b) as-deposited (uncharged) NC films for a range of Nb doping content. c) A plot of the 1st derivative of the Ti K-edge for as-deposited NC films with a range of Nb doping shows the position of the main edge energy.

Spectroelectrochemistry.

The results of *in situ* spectroelectrochemical measurements of film transmittance are reported in terms of the change in Optical Density (ΔOD) of the film upon charging. This metric is a measurement of extinction, baselined to the total extinction of the as-deposited film. The undoped and Nb-TiO_2 NC films darken upon reduction across most of the recorded spectral region, so the ΔOD graphs presented in the main text and below demonstrate positive changes in the extinction of the film upon reduction. There was minor variation in film thickness between different samples, so extinction was normalized with respect to film thickness to enable a quantitative comparison. The conversion from transmittance to normalized ΔOD data is visualized in Figure S6.

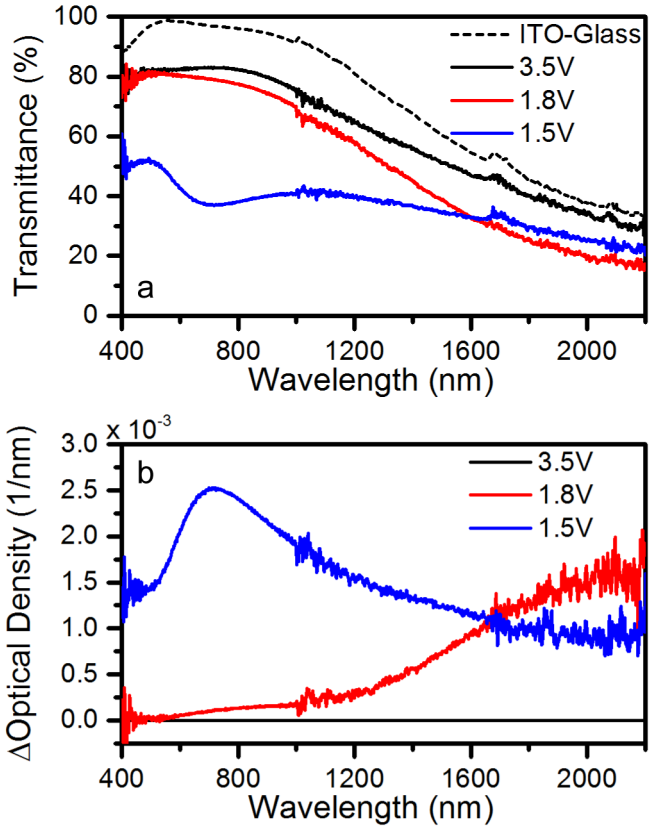

Figure S6. *In situ* spectroelectrochemical data for a 140nm thick 8% Nb-TiO_2 NC film deposited on an ITO-glass substrate, as a) transmittance and b) thickness normalized extinction spectra showing modulation from the fully oxidized state (3.5V). Films were electrochemically cycled in 0.1M LiTFSI in tetraglyme.

Optical switching was compared across a broad range of Nb doping to assess the tunability of the electrochromic effect in these films. All films were within 60 nm of 160nm thickness, and electrochemically cycled following the same methods described for the *in situ* results presented in Figure 4 of the main text. The modulation achieved at each of the four electrochromic modes was compared by measuring the normalized ΔOD at a set of reference wavelengths for all of the measured films. There were no discernable trends in measured ΔOD of the 'Warm' (1.8V upon oxidation, $Li_{0.5}TiO_2$) and 'Dark' (1.5V, $Li_{0.5}TiO_2$) modes with varying Nb doping, but the capacitively reduced 'Cool' mode (1.8V upon reduction, anatase TiO_2) shows positive correlation with Nb content. A plot of ΔOD at three reference NIR wavelengths – 1000nm, 1500nm and 2000nm – for capacitively reduced 1.8V 'Cool' mode films is presented in

Figure S7. There appears to be a maximum in modulation of the NIR extinction for about 7% Nb doping.

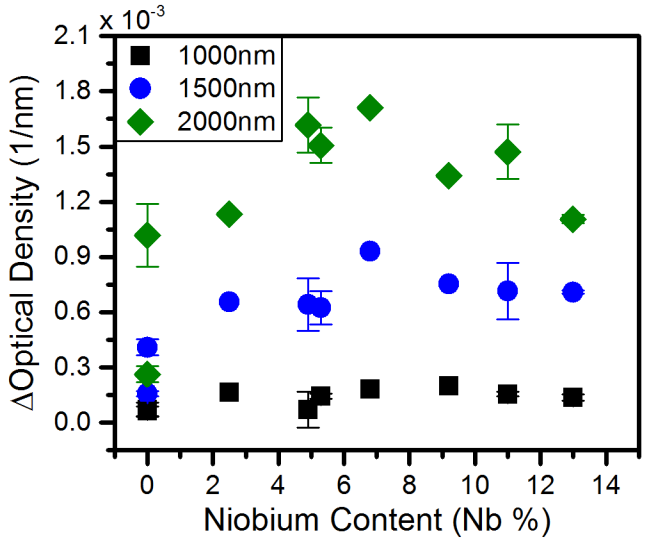

Figure S7. A plot of thickness-normalized ΔOD vs. Nb doping content for NC films capacitively reduced to 1.8V (the 'Cool' mode), shown for three different NIR wavelengths. The error bars represent the standard deviation in ΔOD values for NCs that were prepared in duplicate or triplicate films. The data points without error bars show NCs that were not cast into multiple films to test for error, but they likely demonstrate similar measurement errors.

Mid-IR extinction measurements of the charged NC films were taken with a Bruker Vertex 70 FTIR spectrometer. FTIR spectra of both as deposited (nominally 3.5V) and capacitively reduced films (1.8V upon reduction) were recorded. To avoid oxidation due to air exposure, FTIR spectra were obtained immediately after removing the cell from the glovebox using a rapid transmission-mode scan lasting roughly 2 minutes. Mild oxidation due to air exposure was observed upon air exposure of the air-free cell, so the extinction of the reduced samples is likely lower than would be expected. The TiO_2 film actually lowers the extinction of the substrate and air-free cell, perhaps by decreasing the reflectivity of the naked gold coating on silicon. Thus, to compare the extinction spectra across different doping levels and charge states, all spectra were baselined against the undoped, as deposited TiO_2 NC film. There was significant

variation in film thickness during this experiment, so baselined extinction spectra were then normalized by thickness.

Nb Doping (% Nb)	Thickness (nm)
0%	435
5%	630
7%	1260
13%	1190

$$\text{Normalized Extinction} = \frac{\text{Ext. - Ext. (3.5V, Undoped } TiO_2)}{\text{Thickness / Thickness (Undoped } TiO_2)}$$

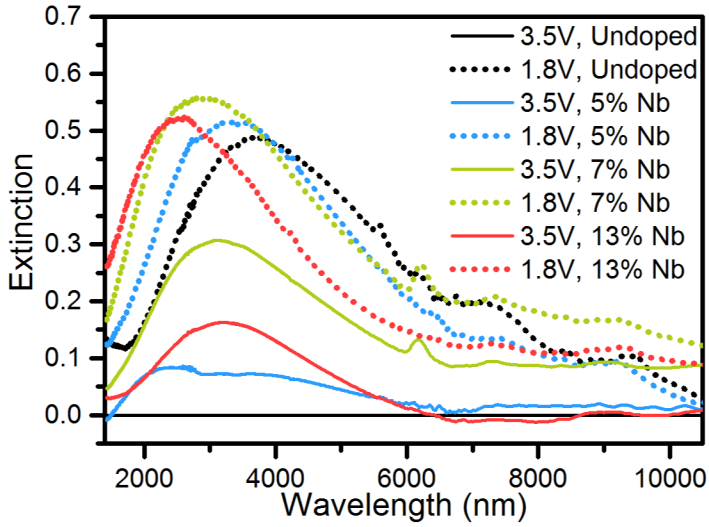

Figure S8. Thickness measurements of *ex situ* charged NC films for transmission FTIR measurements and a comparison of extinction of oxidized and capacitively reduced (1.8 V upon reduction) films for a range of Nb doping content. Spectra were baselined to the oxidized undoped TiO_2 film, and normalized by thickness.

References.

(1) De Trizio, L.; Buonsanti, R.; Schimpf, A. M.; Llordes, A.; Gamelin, D. R.; Simonutti, R.; Milliron, D. J. *Chem. Mater.* **2013**, *25*, 3383.

(2) Dong, A.; Ye, X.; Chen, J.; Kang, Y.; Gordon, T.; Kikkawa, J. M.; Murray, C. B. *J. Am. Chem. Soc.* **2011**, *133*, 998.

(3) Wagemaker, M.; Kearley, G. J.; van Well, A. A.; Mutka, H.; Mulder, F. M. *J. Am. Chem. Soc.* **2003**, *125*, 840.

(4) Bearden, J. A.; Burr, A. F. *Rev. Mod. Phys.* **1967**, *39*, 125.

(5) Marcus, M. A.; MacDowell, A. A.; Celestre, R.; Manceau, A.; Miller, T.; Padmore, H. A.; Sublett, R. E. *J. Synchrotron Rad.* **2004**, *11*, 239.